

Article

# Dynamics Modeling and Motion Simulation of USV/UUV with Linked Underwater Cable

Sung Min Hong <sup>1</sup>, Kyoung Nam Ha <sup>1</sup> and Joon-Young Kim <sup>2,\*</sup><sup>1</sup> Precision Mechanical Process and Control R&D Group, Korea Institute of Industrial Technology, Busan 46041, Korea; hsm3087@kitech.re.kr (S.M.H.); Ovincent@kitech.re.kr (K.N.H.)<sup>2</sup> Department of Ocean Advanced Material Convergence Engineering, Korea Maritime and Ocean University, Busan 49112, Korea

\* Correspondence: jykim@kmou.ac.kr; Tel.: +82-10-6462-3485

Received: 27 March 2020; Accepted: 25 April 2020; Published: 30 April 2020



**Abstract:** This paper describes a study on the dynamic modeling and the motion simulation of an unmanned ocean platform to overcome the limitations of existing unmanned ocean platforms for ocean exploration. The proposed unmanned ocean vehicle combines an unmanned surface vehicle and unmanned underwater vehicle with an underwater cable. This platform is connected by underwater cable, and the forces generated in each platform can influence each other's dynamic motion. Therefore, before developing and operating an unmanned ocean platform, it is necessary to derive a dynamic equation and analyze dynamic behavior using it. In this paper, Newton's second law and lumped-mass method are used to derive the equations of motion of unmanned surface vehicle, unmanned underwater vehicle, and underwater cable. As the underwater cable among the components of the unmanned ocean platform is expected to affect the motion of unmanned surface vehicle and unmanned underwater vehicle, the similarity of modeling is described by comparing with the cable modeling results and the experimental data. Finally, we constructed a dynamic simulator using Matlab and Simulink, and analyzed the dynamic behavior of the unmanned ocean platform through open-loop simulation.

**Keywords:** unmanned surface vehicle (USV); unmanned underwater vehicle (UUV); underwater cable; unmanned ocean platform; dynamic modeling & simulation

## 1. Introduction

Among various studies related to marine development, marine exploration is a fundamental physical exploration that is needed for multiple purposes, such as resource and energy development and management, navigation safety, and military operations. Marine exploration is being used directly for engineering purposes such as marine civil engineering and offshore plant installations through the marine development phases, ranging from the initial exploration stage of resource development to the production of equipment, the changes of terrain during the production process [1], but, if the undersea topography or depth of water information is not accurate, it may cause damage such as stranding of ships, damage to underwater optical cables, and damage to offshore structures. Accordingly, marine exploration is necessary and with the development of science and technology along with the necessity, studies of marine exploration using unmanned robot technology in an underwater environment that replaces existing ships or humans, are actively being carried out. Thus research on unmanned marine robots has been conducted for a long time and various types of platforms are being developed and operated due to necessities such as marine exploration. These include unmanned surface vehicles (USVs), autonomous underwater vehicles (AUVs), remotely operated vehicles (ROVs),

underwater gliders (UGs) and towed-systems. Also, studies and equipment development for a deep tow survey system are being carried out for precise exploration of seabed topography [2].

Recently, an unmanned ocean platform has been developed as a combination of USV and ROV or USV and a towed-system, as shown in Figure 1 below. These platforms are being developed to reduce costs and manpower incurred when using a ship [3–6].



**Figure 1.** Combined Unmanned Ocean Platform: (a) Inspector USV with H300V; (b) Halcyon-Seaeye; (c) AQS-24 with Spartan; (d) Mine Hunting Unmanned Surface Vehicle (MHU).

As shown in Figure 1, it is difficult to explore a large area due to the operating characteristics of a ROV that combines an USV and a ROV. Also, the towed-system can quickly explore a large area, but it is difficult to obtain accurate location information of the exploration area and to predict the towed-system kinetic performance under water. Therefore, this study proposes a platform that combines an USV and an UUV to overcome the disadvantages of the above platform. The proposed platform is based on an USV like the similar platform. The platform for underwater exploration is a torpedo-shaped UUV. This type of platform has the advantage of being able to quickly explore a larger area than the ROV. Besides, it is equipped with USV's GPS and USBL to reduce the navigation error, which is a disadvantage of the existing AUVs, and to find the exact location of the exploration area. The UUV connected to the underwater cable is equipped with a propeller, allowing position control, which makes high-speed driving for stable towed system operation unnecessary, and can check information in real-time through the underwater cable.

In this study, a dynamic analysis of the proposed platform was performed through simulation before platform development. The existing studies mainly analyzed the motion between the ROV and the underwater cable while the USV was fixed or analyzed the motion changes of the underwater cable according to the USV motion at high speed [7–13], but, the unmanned ocean platform proposed in this study performs marine exploration while the USV and UUV move simultaneously. Therefore, it is necessary to analyze the effect of the underwater cable on the movement of the USV and UUV while the platform is moving.

In this study, motion equations for the USV, UUV and underwater cable were derived, and the motion performance of the unmanned ocean platform was verified through simulation. The motion equations of the USV and UUV were derived using Newton's second law, and mathematical modeling of underwater cables was performed using the lumped-mass method [14–20]. As mentioned earlier, the force generated by underwater cables is an important factor influencing the USV and UUV movements. Therefore, in this study, the behavior of the actual underwater cable was performed in the presence of current. The accuracy of modeling was confirmed by comparing the experimental values with those calculated through modeling and simulation.

Also, the motion equations derived for each platform and the connection between each platform were considered to derive the overall motion equation for the unmanned ocean platform. In addition, a simulator for analyzing the motion performance of the unmanned ocean platform was constructed using the derived equations of motion and Matlab and Simulink. Through open-loop simulation, the motion performance of the unmanned ocean platform was confirmed. Through the simulation results, matters to be considered when operating the unmanned ocean platform were described.

## 2. Dynamics Modeling

This section describes the process of deriving the equations of motion for the analysis of the motion performance of the unmanned ocean platform, as shown in Figure 2. The unmanned ocean platform is composed of an USV, an UUV and underwater cable and the dynamic equations for each are derived.

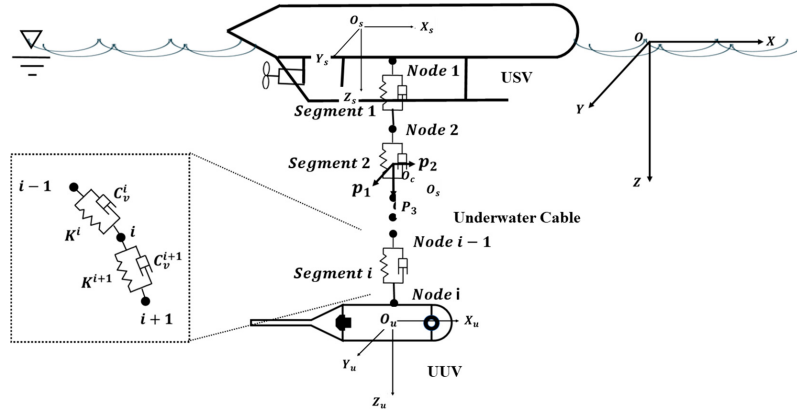


**Figure 2.** Schematic of the Unmanned Ocean Platform.

### 2.1. Notation and Coordinate System

The notation used to derive the equation of motion follows SNAME [15], as shown in Table 1, and USV, UUV and underwater cable are classified using subscripts s, f and c. The position and orientation were defined in the Earth-fixed frame and linear and angular velocity, forces and moments are defined in the body-fixed reference frame and local frame. The orientation of the marine robot can be expressed using Euler angles or quaternions, as shown in Table 1 below. In this paper, it is assumed that singularity that can occur by using Euler angles, that is when the pitch angle becomes 90 degrees, does not occur, and Euler angles are used.

**Table 1.** Notation used for the USV and UUV.

Degree of Freedom	Forces and Moments	Linear and Angular Velocities	Position and Orientation
Translational Motion	Surge (x-axis)	$X_i$	$x_i$
	Sway (y-axis)	$Y_i$	$y_i$
	Heave (z-axis)	$Z_i$	$z_i$
Rotational Motion	Roll (x-axis)	$K_i$	$\phi_k$
	Pitch (y-axis)	$M_i$	$\theta_k$
	Yaw (z-axis)	$N_i$	$\psi_k$

where,  $i = \{s, f\} = \{\text{USV}, \text{UUV}\}$  and  $k = \{s, f, c\} = \{\text{USV}, \text{UUV}, \text{Cable}\}$ .

To describe the motion of the unmanned ocean platform, on Earth-fixed frame ( $O, X, Y, Z$ ), two body-fixed reference frames, and one local frame are required. Figure 2 shows the schematic of the unmanned ocean platform and the coordinate system set for each platform. The body-fixed reference frames ( $O_s, X_s, Y_s, Z_s$ ) and ( $O_u, X_u, Y_u, Z_u$ ) represent the coordinate systems of the USV and UUV, respectively, and were set to coincide with the center of gravity of the USV and UUV. A local frame ( $P_1, P_2, P_3$ ) was coincided for each segment of the underwater cable. The body-fixed reference frame defines in USV and UUV determined the x-axis in the forward direction and the y-axis in the starboard direction and the z-axis according to the right-hand rule. Also, each axis of the local frame defined in the underwater cable means a normal vector, a bi-normal vector, and a tangent vector.

## 2.2. Linear and Angular Velocity Transformation

Coordinate transformation is needed to express the linear and angular velocity defined in the body-fixed reference frame as an Earth-fixed frame. The matrix that converts the linear and angular velocity defined in the body-fixed reference frame to the Earth-fixed frame using is as shown in equations (1) and (2) below:

$$R_1 = \begin{pmatrix} c\psi_k c\theta_k & -s\psi_k c\theta_k + c\psi_k s\theta_k s\phi_k & s\psi_k s\phi_k + c\psi_k c\phi_k s\theta_k \\ s\psi_k c\theta_k & c\psi_k c\phi_k + s\phi_k s\theta_k s\psi_k & -c\psi_k s\phi_k + s\theta_k s\psi_k c\phi_k \\ -s\theta_k & c\theta_k s\phi_k & c\theta_k c\phi_k \end{pmatrix} \quad (1)$$

$$R_2 = \begin{pmatrix} 1 & t\theta_k s\phi_k & c\phi_k t\theta_k \\ 0 & c\phi_k & -s\phi_k \\ 0 & s\phi_k / c\theta_k & c\phi_k / c\theta_k \end{pmatrix} \quad (2)$$

## 2.3. 6-DOF Dynamic Equations of Motion of Marine Vehicle

In this paper, the 6-DOF motion equation of the USV and UUV to be derived is generally expressed as the following Equation (3) [15]:

$$\mathbf{M}\mathbf{v} + \mathbf{C}(\mathbf{v})\mathbf{v} + \mathbf{D}(\mathbf{v})\mathbf{v} + \mathbf{g}(\eta) = \boldsymbol{\tau} \quad (3)$$

where,  $\mathbf{v} = [\mathbf{u}, \mathbf{v}, \mathbf{w}, \mathbf{p}, \mathbf{q}, \mathbf{r}]^T$ ,  $\eta = [\mathbf{x}, \mathbf{y}, \mathbf{z}, \phi, \theta, \psi]^T$ ,  $\boldsymbol{\tau} = [\mathbf{X}, \mathbf{Y}, \mathbf{Z}, \mathbf{K}, \mathbf{M}, \mathbf{N}]^T$ . Equation (3) is developed using the Newtonian and Lagrangian methods and is expressed in vector form. Each vector included in the equation is shown in Appendix A.

$\mathbf{M}$ ,  $\mathbf{C}(\mathbf{v})$ ,  $\mathbf{D}(\mathbf{v})$ ,  $\mathbf{g}(\eta)$ ,  $\boldsymbol{\tau}$  included in Equation (3) represent the inertia matrix, Coriolis and centripetal terms matrix, damping matrix, gravitational forces and moments and control inputs, respectively. The equations of motion of the USV and UUV, which will be introduced below, were developed and used in the study using Equation (3) along with several assumptions.

## 2.4. USV Modeling

The conceptual diagram of the USV to be developed in this study is shown in Figure 3. The USV is equipped with two thrusters at the rear, and the coordinate system is set.

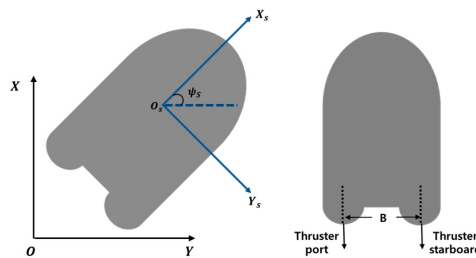


**Figure 3.** Conceptual diagram and coordinate system of USV

The USV 3-DOF equation can be expressed considering the assumptions below:

- Homogeneous mass distribution and xz-plane symmetry
- The heave, roll and pitch modes can be neglected
- The damping matrix element can ignore the first order higher-order term

The transformation matrix for expressing the linear and angular velocity of the USV in the Earth-fixed frame can be expressed using the previously defined matrices (1) and (2).

Therefore, the kinematics of USV is expressed using Equation (4) above, while the simplified 3-DOF equation for USV is given by Equation (5):

$$\begin{aligned} x_s &= u_s \cos \psi_s - v_s \sin \psi_s \\ y_s &= u_s \sin \psi_s + v_s \cos \psi_s \\ \psi_s &= r_s \end{aligned} \quad (4)$$

$$\begin{aligned} (m_s - X_{u_s})u_s - (m_s - Y_v)v_s r_s - (X_{u_s} + X_{uu_s}|u_s|)u_s &= X_s \\ (m_s - Y_v)v_s + (m_s - X_{u_s})u_s r_s - (Y_{v_s} + Y_{vv_s}|v_s|)v_s &= Y_s \\ (I_{Z_s} - N_{r_s})r_s - (Y_{v_s} + X_{u_s})u_s v_s - (N_{r_s} + N_{rr_s}|r_s|)r_s &= N_s \end{aligned} \quad (5)$$

where,  $m_s$  is mass,  $X_{u_s}$ ,  $Y_{v_s}$ ,  $N_{r_s}$ ,  $X_{u_s}$ ,  $X_{uu_s}$ ,  $Y_{v_s}$ ,  $Y_{vv_s}$ ,  $N_{r_s}$ ,  $N_{rr_s}$  are hydrodynamic coefficients,  $X_s$ ,  $Y_s$ ,  $N_s$  are external forces.

The right side of Equation (5) represents the external force acting on the USV. In this study, thrust force, wind force, and current were considered as external forces.

#### 2.4.1. Thrust Force Acting on the USV

The thrusters used in this study are MINN KOTA thrusters [21], not omnidirectional thrusters. As shown in Figure 3, the control force and moment can be defined by the following Equation (6) considering the arrangement of the thrust:

$$\tau_{thrust_s} = \begin{bmatrix} X_{thrust_s} \\ N_{thrust_s} \end{bmatrix} = \begin{bmatrix} T_{port_s} + T_{stbd_s} \\ (T_{port_s} - T_{stbd_s}) \times \frac{B}{2} \end{bmatrix} \quad (6)$$

In order to apply thrust of actual thrusters to the simulation, forward and reverse thrust tests of thrusters mounted on the USV were performed. Thrust test was carried out at the Marine Robotics Center of the Korea Institute of Industrial Technology (KITECH). As, shown in Figure 4, below, a tension meter was mounted on the head and the rear on the USV and results of the thrust measurement experiment. The dead zone of the thruster was about 1.6 ~ 3.2 V. The thrust force is nonlinear but can be used by linearizing the relationship between thrust force and control voltage. The maximum forward thrust was 29.12 kgf, and the maximum reverse thrust was 13.83 kgf.

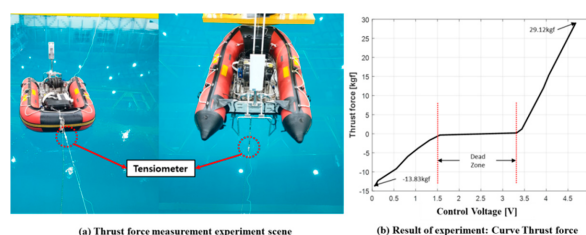


**Figure 4.** Thrust force measurement of the USV.

#### 2.4.2. Wind Load

Disturbances acting on a USV include wave load, current load, and wind load. Such disturbances can cause drift motion of the USV. These disturbances need to be taken into consideration to more accurately describe the motion. In this study, the load due to the waves was not considered because the load caused by the wind was more dominant than the load caused by the waves under the same sea conditions. The magnitude of the force and moment acting on the USV was calculated using the Fossen wind load model [15]. The following Equation (7) shows the force and moment due to wind load:

$$\tau_{wind_s} = \begin{bmatrix} X_{wind} \\ Y_{wind} \\ N_{wind} \end{bmatrix} = \begin{bmatrix} \frac{1}{2} C_X(\gamma_R) \rho_w V_R^2 A_T \\ \frac{1}{2} C_Y(\gamma_R) \rho_w V_R^2 A_L \\ \frac{1}{2} C_N(\gamma_R) \rho_w V_R^2 A_L L \end{bmatrix} \quad (7)$$

$$C_X(\psi_R) = -c_x \cos(\psi_R), C_Y(\psi_R) = c_y \sin(\psi_R), C_N(\psi_R) = c_z \sin(2\psi_R) \quad (8)$$

$$C_x \in (0.5, 0.9), C_y \in (0.7, 0.95), C_z \in (0.05, 0.2) \quad (9)$$

where,  $C_X$ ,  $C_Y$ ,  $C_N$  are wind load coefficients, and  $\rho_w$  is the air density.  $A_T$ ,  $A_L$ ,  $L$  refer to the frontal projected area, the lateral projected area, and the horizontal length from the front end of the USV to the end of aft end, respectively.

#### 2.4.3. Current Load

Due to a variety of factors such as wind, waves or ocean temperature differences, currents, and so on, very sophisticated forms of current can occur in irregular shapes, complicating the model's precision mathematically to account for effects of current. Therefore, it is common to model current in marine environment using the first Gauss-Markov process [15]. In general, the equation of motion of a USV considering the effects of a current instead of directly applying the forces and moments applied to the hull by the current directly to the equation of motion replaces the relative velocity of the current and the USV to a previously derived motion equation. It is used as a method.

The current velocity ( $V_c$ ) in earth-fixed frame defined as shown in Figure 5 is the body-fixed reference frame of the USV and can be converted as shown in Equation (10) below:

$$\begin{aligned} u_{cs} &= V_c \cos(\beta - \psi_s) \\ v_{cs} &= V_c \sin(\beta - \psi_s) \end{aligned} \quad (10)$$

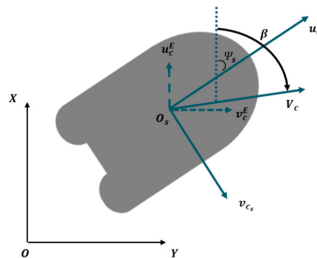


**Figure 5.** Defined Velocity ( $V_c$ ) and direction ( $\beta$ ) of the current

#### 2.5. UUV Modeling

The UUV, which performs marine exploration mission on a unmanned ocean platform, has the shape of a torpedo, as shown in Figure 6 below. Also, two rear thrusters and one thruster are arranged in the Y-axis direction.

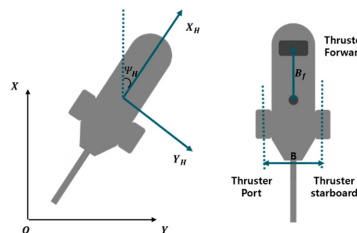


**Figure 6.** Conceptual diagram and coordinate system of the UUV.

To describe the behavior of an UUV in water, both rigid-body dynamics and fluid dynamics should be considered. In particular, in terms of fluid dynamics, it is assumed that "force and moment due to a fluid acting on a rigid body can be linearly superimposed" can be applies to rigid body dynamics. The equation of motion of the UUV developed along this assumption is shown in Equation (11).

By substituting each matrix demonstrated in Appendix A in Equation (11), the 6-DOF nonlinear motion equation of UUV can be developed as follows:

$$\begin{aligned} m_f[u_f - v_f r_f + w_f q_f - x_{g_f}(q_f^2 + r_f^2) + y_{g_f}(p_f q_f - r_f) + z_{g_f}(p_f r_f + q_f)] &= \Sigma X_f \\ m_f[v_f - w_f p_f + u_f r_f - y_{g_f}(r_f^2 + p_f^2) + z_{g_f}(q_f r_f - p_f) + x_{g_f}(p_f q_f + r_f)] &= \Sigma Y_f \\ m_f[w_f - v_f r_f + v_f q_f - z_{g_f}(p_f^2 + q_f^2) + x_{g_f}(r_f p_f - q_f) + y_{g_f}(r_f q_f + p_f)] &= \Sigma Z_f \\ I_{x_f} p_f + (I_{z_f} - I_{y_f}) q_f r_f + m_f[y_{g_f}(w_f - u_f q_f + v_f p_f) - z_{g_f}(w_f - w_f p_f + v_f r_f)] &= \Sigma K_f \\ I_{y_f} q_f + (I_{x_f} - I_{z_f}) r_f p_f + m_f[z_{g_f}(u_f - v_f r_f + w_f q_f) - x_{g_f}(w_f - u_f q_f + v_f p_f)] &= \Sigma M_f \\ I_{z_f} r_f + (I_{y_f} - I_{x_f}) p_f q_f + m_f[x_{g_f}(v_f - w_f p_f + u_f r_f) - y_{g_f}(u_f - v_f r_f + w_f q_f)] &= \Sigma N_f \end{aligned} \quad (11)$$

where  $m_f$  is the mass of the UUV,  $[I_{x_f}, I_{y_f}, I_{z_f}]^T$  is the mass secondary moment in the X, Y, Z axis direction, and  $[x_{g_f}, y_{g_f}, z_{g_f}]^T$  is the center of gravity. The right side represents the sum of forces and moments due to hydrodynamic forces and moments, disturbance, thrust forces and moments.

The influence of ocean environment on the UUV is less than that by disturbance such as waves and winds considering that the UUV is operated in water. Therefore, in this study, it was assumed that the force and moment due to currents were the only disturbances. In this case, influence of the current was the same as the current considered in the disturbance of the USV described above. The current expressed in the UUV body-fixed reference frame is as follows:

$$\begin{aligned} u_{c_f} &= V_c \cos(\beta - \psi_f) \\ v_{c_f} &= V_c \sin(\beta - \psi_f) \end{aligned} \quad (12)$$

### Thrust Force Acting on the UUV

A Technadyne Model 300 thruster will be used for the UUV [22]. Therefore, it was intended to include it in the UUV motion equation external force term. The thrust force curve, according to the control voltage, was found through thrust test, as shown in the Figure 7 below, and Equation (13) represents the external force included in the right side of the equation of motion. The two thrusters mounted on the rear have a force in the forward direction of the UUV, and the thruster in front generate a rotating force in the z-axis direction:

$$\tau_{thrust_f} = \begin{bmatrix} X_{thrust_f} \\ N_{thrust_f} \end{bmatrix} = \begin{bmatrix} T_{port_f} + T_{stbd_f} \\ T_{forward_f} \times B_f \end{bmatrix} \quad (13)$$

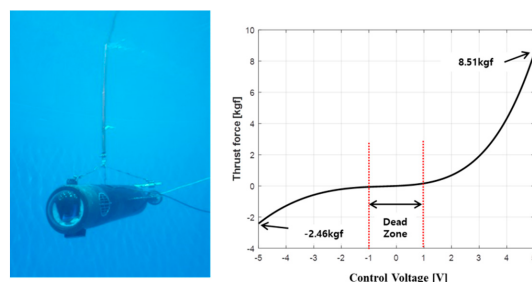


Figure 7. Thrust force measurement of the UUV.

## 2.6. Underwater Cable Modeling and Experimental Validation

### 2.6.1. Underwater Cable Modeling

The cables are considered small rigid segments instead of continuous non-rigid members. Each segment has a local frame and expresses the motion for each segment using an individual coordinate system as an equation and applies it to the whole system. The following assumptions are made to derive the equation of motion of the underwater cable:

- The umbilical cable is incompressible.
- The cable surface is relatively smooth, ignoring the attachments on the cable.
- The bending stiffness of the cable is ignored. The umbilical cable can only resist the tension force, but not the bending moment and the compression force.
- The torsional rigidity and the quality of cable point rotation effect, which do not consider the torque, are ignored.

As shown in Figure 8, the underwater cable consists of  $N$  segments and  $N+1$  nodes. Also, a local frame is located at the center of mass of each segment. The tension, damping, and hydrodynamic drag forces acting on the cable are calculated in the local frame and these forces act as constraints on the motion of adjacent nodes.

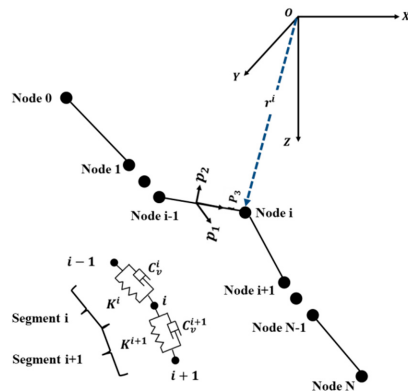


**Figure 8.** Illustration of the discrete representation of the underwater cable.

The orientation of each segment can be expressed using an Euler angle. Since we do not consider torsion of the cable along the Z-axis, we can define the matrix  $R_{IB}^n$  for converting from the local frame to the Earth-fixed frame using matrix  $R_1$  defined above:

$$R_{EB}^n = \begin{bmatrix} c\theta_c^n & s\theta_c^n s\phi_c^n & c\phi_c^n s\theta_c^n \\ 0 & c\phi_c^n & -s\phi_c^n \\ -s\theta_c^n & c\theta_c^n s\phi_c^n & c\theta_c^n c\phi_c^n \end{bmatrix} \quad (14)$$

The Euler angles included in Equation (14) can be calculated as follows, considering the position of the cable node:

$$\theta_c^n = \text{atan2}(r_X^n - r_X^{n-1}, r_Z^n - r_Z^{n-1}) \quad (15)$$

If  $c\theta_c^n > s\theta_c^n$ :

$$\phi_c^n = \tan^{-1} \left( -\left(r_Y^n - r_Y^{n-1}\right), \frac{r_Z^n - r_Z^{n-1}}{c\theta_c^n} \right) \quad (16)$$

If  $c\theta_c^n < s\theta_c^n$ :

$$\phi_c^n = \tan^{-1} \left( -\left(r_Y^n - r_Y^{n-1}\right), \frac{r_X^n - r_X^{n-1}}{s\theta_c^n} \right) \quad (17)$$

According to the lumped mass method, the internal force generated in the underwater cable includes tension and damping while the external force includes gravity, buoyancy, and drag force. It can be defined as described below.

The method of calculating and applying tensile force to the three axes that occur due to elastic movement of the cable among forces acting inside is shown in previous study [23]. From this method, the tension acting on the tangential element can be expressed as a linear function as follows (18) according to Hooke's law:

$$T^n = EA\epsilon^n, \epsilon^n = \frac{l^n - l_0^n}{l_0^n} \quad (18)$$

where  $l_0^n$  is the not deformed  $n$ -th segment,  $A$  is the cross-sectional area of the cable, and  $E$  is the modulus of elasticity. The axial force generated by the damping between tangential strains and damping force can be defined with the following Equation (19):

$$P^n = C_v(V_q^n - V_q^{n-1}) \quad (19)$$

In equation (x),  $V_q^n$  represents the speed in the tangential direction of the  $n$ -th segment and  $C_v$  is a damping coefficient.

The external force acting on the underwater cable includes hydrodynamic force, weight, and buoyancy, and fluid resistance acting on the underwater cable that originates from the water or cable movement. Assuming that the radius and length of the underwater cable and the exposed cable outside the water are almost free, force due to waves can be ignored [12,24].

Therefore, waves are not modeled. Only a constant current is assumed. Thus, water surrounding the cable is not accelerated. This means that there is no dynamic pressure gradient around the water. The Froude-Krilov force is zero. The force generated by the relative velocity of the fluid can be expressed with Equation (20) below:

$$\begin{aligned} D_{p1}^n &= -\frac{1}{2}\rho_w C_d d_c l_0^n f_p |V^n|^2 \frac{V_{p1}^n}{\sqrt{(V_{p1}^n)^2 + (V_{p2}^n)^2}} \\ D_{p2}^n &= -\frac{1}{2}\rho_w C_d d_c l_0^n f_p |V^n|^2 \frac{V_{p2}^n}{\sqrt{(V_{p1}^n)^2 + (V_{p2}^n)^2}} \\ D_{p3}^n &= -sgn(v_q^n) \frac{1}{2}\rho_w C_d d_c l_0^n f_{p3} |V^n|^2 \end{aligned} \quad (20)$$

where  $D_{p1}^n$ ,  $D_{p2}^n$ ,  $D_{p3}^n$  represent the kinematic forces for each axis expressed in the local frame.  $\rho_w$ ,  $C_d$ ,  $d_c$ ,  $V^n$  denote the density of water, resistance coefficient, cable diameter, and relative velocity of the cable and the fluid, respectively. Also,  $f_p$ ,  $f_{p3}$  denote the loading function for determining the drag coefficient. They are expressed by the following Equation (21) [25]:

$$\begin{aligned} f_p &= 0.5 - 0.1 \cos(\eta) + 0.1 \sin(\eta) - 0.4 \cos(2\eta) - 0.11 \sin(2\eta) \\ f_{p3} &= 0.01(2.008 - 0.3858\eta + 1.9159\eta^2 - 4.1615\eta^3 + 3.5064\eta^4 - 1.1873\eta^5) \end{aligned} \quad (21)$$

where  $\eta$  is expressed in radians, and  $0 \leq \eta \leq \frac{1}{2}$ .

The hydrodynamic force acting on each node shares force acting on adjacent segments. It has a value of half.

Mass and buoyancy can be obtained with the following Equation (22):

$$\begin{aligned} m_c^n &= \rho_c g V_c^n \\ B_c^n &= \rho_w g V_c^n \end{aligned} \quad (22)$$

where,  $\rho_c$ ,  $g$ ,  $V_c^n$  denote cable density, gravitational acceleration, and volume of the segment.

An object moving in water is subjected to an additional mass by the fluid. For the tangential direction, the added mass is not considered. The mass matrix of each segment is as follows:

$$M_B^n = \begin{bmatrix} m_c^n + m_a^n & 0 & 0 \\ 0 & m_c^n + m_a^n & 0 \\ 0 & 0 & m_c^n \end{bmatrix} \quad (23)$$

where  $m_a^n$  is the added mass of the cylindrical cable element as given by [26,27].

The mass matrix can be expressed in the earth-fixed frame using transformation matrix defined above. It can be expressed by the following Equation (24):

$$M_E^n = \frac{1}{2} R_{EB}^n M_B^n R_{EB}^{nT} + \frac{1}{2} R_{EB}^{n+1} M_B^{n+1} R_{EB}^{n+1T} \quad (24)$$

Using the force acting on each segment and the second law of Newton, we can derive the equation of motion of underwater cable as follows:

$$M_E^{n''n} = (T^{n+1} + P^{n+1}) - (T^n + P^n) + \frac{1}{2}(D^n + D^{n+1} + m_c^n + m_c^{n+1}) - \frac{1}{2}(B^n + B^{n+1}) \quad (25)$$

## 2.6.2. Underwater Cable Verification

In order to verify the validity of dynamics modeling of the underwater cable, simulation were carried out under the assumption there presence of current. Also, on end of the underwater cable was fixed, and the other side considered weight and inertia matrix of the UUV.

Simulation result in comparison with results of experiments performed in the water tank confirmed the validity of dynamics modelling of the underwater cable. The characteristics of the underwater cable used in the simulation are shown in Table 2 below.

**Table 2.** Specification of Underwater Cable.

Parameter	Value
Cable diameter	0.025 m
Cable density	3121 kg/m <sup>3</sup>
Cable drag coefficient	2.5
Cable damping coefficient	100 Ns
Effective modulus of elasticity	7.5 × 10 <sup>6</sup> GPa
Total cable length	3 m
Number of Cable nodes	20

The simulation was performed by changing the current from 0 to 1 m/s. Results are shown in Figure 9. As the speed of the current increased, the cable was pushed backward. Tension acting on the cable at the initial position acted the most and converged with time, reaching an equilibrium state by the elastic modulus included in the cable motion equation.

Figure 10 below shows a scheme of the experiment performed to measure the tension acting on the cable and the angle of the cable.

Figure 11 shows the results of an actual experiment. The lay-back angle of the cable was measured using a high-speed camera. In addition, the tension was measured using a tension meter installed at the end of the cable.

Table 3 shows the simulation and experimental results. The difference in the result for the tension was 0.03 kgf to 1.67 kgf, and the lay-back angle was 0.18 deg to 2.56 deg. Although the difference of each result is visible, it can be confirmed that the magnitude of the value is not large, and the movement tendency of the cable is similarly expressed. Therefore, it was confirmed that the cable motion equation derived above was valid.

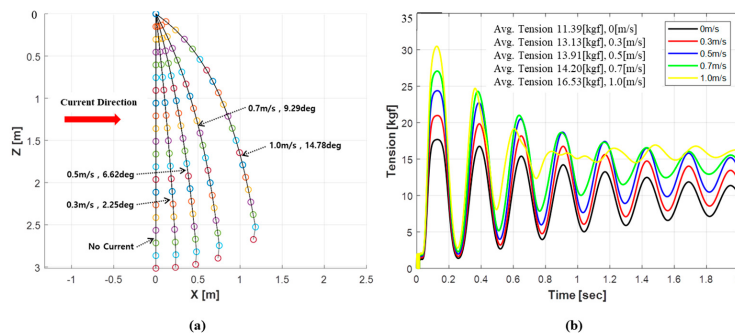


**Figure 9.** Simulation result of cable motion with current: (a) Cable lay-back angle change according to current (0 m/s to 1 m/s); (b) Force acting on the last node of the cable.



**Figure 10.** Scheme of water tank test for measuring force.

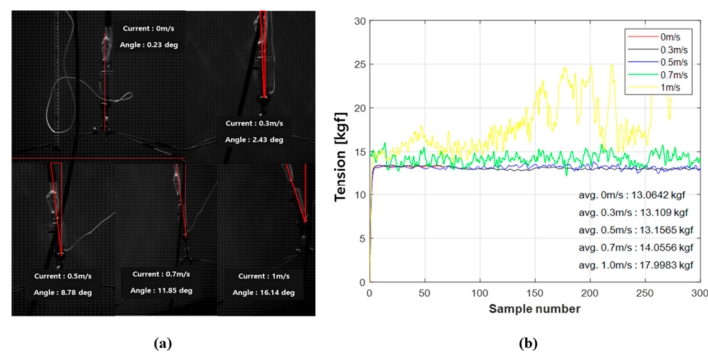


**Figure 11.** Experiment result of cable motion with current: (a) Cable lay-back angle according to current (0 m/s to 1 m/s); (b) Force acting on the last node of the cable.

**Table 3.** Comparison of cable motion simulation results and experiment values.

	Current Velocity	Simulation	Experiment
Tension [kgf]	0 m/s	11.39	13.06
	0.3 m/s	13.13	13.10
	0.5 m/s	13.91	13.15
	0.7 m/s	14.20	14.05
	1.0 m/s	16.53	17.99
Lay-back Angle [deg]	0 m/s	0	0.23
	0.3 m/s	2.25	2.43
	0.5 m/s	6.62	8.78
	0.7 m/s	9.29	11.85
	1.0 m/s	14.78	16.14

### 3. Full Unmanned Ocean Platform Model

#### 3.1. Boundary Conditions

Boundary conditions must be placed at both ends of the underwater cable. Also, one node was added to each end of the underwater cable. The added node has the position and velocity of the USV and UUV. In other words, the added node is dependent on the position and velocity of the USV and UUV, which means that the cable shape and internal tension changes occur. Therefore, the position and velocity of the node added at the first and last of the underwater cable can be expressed as a function of the node number and time:

$$\begin{aligned} x_c(1, t) &= x_s, \quad y_c(1, t) = y_s, \quad z_c(1, t) = z_s = 0 \\ x_c(n+1, t) &= x_f, \quad y_c(n+1, t) = y_f, \quad z_c(n+1, t) = z_f \end{aligned} \quad (26)$$

#### 3.2. Interaction between the USV, UUV and Underwater Cable

As mentioned earlier, to solve the motion equation of the cable, the position and velocity of the USV and UUV must be set as the two boundary values, respectively. Then, it has a circulation structure that applies the force calculated through cable analysis of the USV and UUV.

The interaction between the USV, UUV and underwater cable can be described by the following equations (27) and (28):

$$\begin{aligned} u_1 &= R_{1(\psi_s)}(v_{1_s} + v_{2_s} \times r_{c_s}) \\ r_1 &= R_{1(\psi_s)}r_{c_s} \end{aligned} \quad (27)$$

$$\begin{aligned} u_{n+1} &= R_{1(\theta_f \phi_f \psi_f)}(v_{1_f} + v_{2_f} \times r_{c_f}) \\ r_{n+1} &= R_{1(\theta_f \phi_f \psi_f)}r_{c_f} \end{aligned} \quad (28)$$

where  $R_{1(\psi_s)}$ ,  $R_{1(\theta_f \phi_f \psi_f)}$  is the transformation matrix,  $v_{1_s} = [u_s, v_s]^T$ ,  $v_{2_s} = r_f$ ,  $v_{1_f} = [u_f, v_f, w_f]^T$ ,  $v_{2_f} = [p_f, q_f, r_f]^T$  and  $r_{c_s}, r_{c_f}$  are the position vector of the cable's tying point on the USV and UUV.

Also, the force by the cable expressed in the Earth-fixed frame needs to be represented by the body-fixed reference frame of USV and UUV:

$$\tau_{cable_s} = \begin{bmatrix} F_{scable} \\ M_{scable} \end{bmatrix} = \begin{bmatrix} -R_{1(\psi_s)}^{-1}T_1 \\ r_{c_s} \times (-R_{1(\psi_s)}^{-1}T_1) \end{bmatrix} \quad (29)$$

$$\tau_{cable_f} = \begin{bmatrix} F_{fcable} \\ M_{fcable} \end{bmatrix} = \begin{bmatrix} -R_{1(\theta_f \phi_f \psi_f)}^{-1}T_{n+1} \\ r_{c_f} \times (-R_{1(\theta_f \phi_f \psi_f)}^{-1}T_{n+1}) \end{bmatrix} \quad (30)$$

Considering all of the abovementioned forces acting on the USV and UUV, we can express the vector form of the dynamic model of the USV and UUV using the following equations (31) and (32):

$$M_s v_{rs} + C_s(v_{rs})v_{rs} + D_s(v_{rs})v_{rs} = \tau_{thrust_s} + \tau_{cable_s} + \tau_{wind_s} \quad (31)$$

$$M_f v_{rf} + C_f(v_{rf})v_{rf} + D_f(v_{rf})v_{rf} + g_f(\eta_f) = \tau_{thrust_f} + \tau_{cable_f} \quad (32)$$

The notations expressed in equations (29) and (30) can be found in the process of developing the equation of motion above. Also,  $v_r$  means the relative velocity vector considering the current.

### 4. Dynamic Model Simulation

A set of coupled differential equation of the unmanned ocean platform can be solved simultaneously with dynamic equilibrium at each time step. The position and velocity calculated at each step are used as initial values for the next step calculation. These governing equations are integrated by using the

4th Runge-Kutta method. Figure 12 shows the flow chart for solving the equation of motion of the unmanned ocean platform.

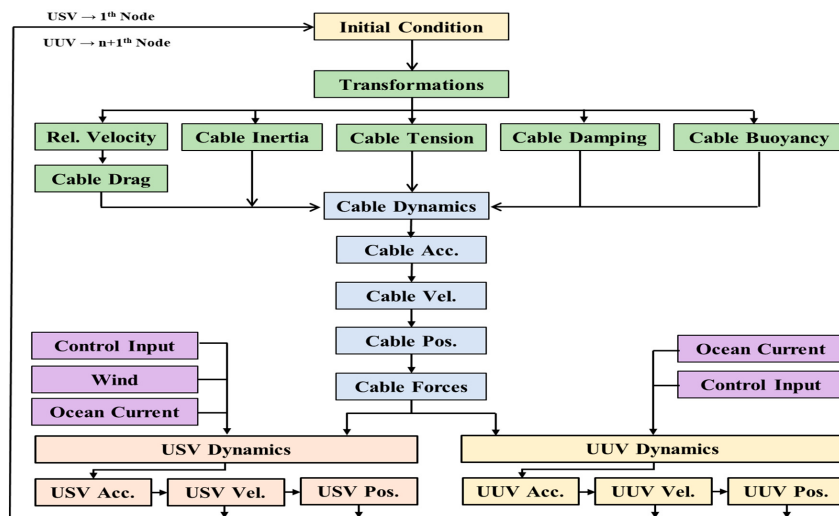


**Figure 12.** Flow chart of the unmanned ocean platform motion simulation.

Table 4 below shows the parameters of USV and UUV required for performing the simulation. The underwater cable parameters are shown in Table 2. In addition to the parameters shown in Table 4, parameters such as hydrodynamic coefficients were simulated by referring to the coefficients of the existing platform with similar specifications of the platform to be developed in this study [19,28]. Simulation was performed using Matlab and Simulink. The fixed step size for analysis was set to 0.001 s. In this paper, the following open-loop simulations were performed, and the results are described.

**Table 4.** The parameters for the simulation.

Parameter	Unit	Value
<b>USV parameters</b>		
Length	m	3
Breadth	m	1.82
Mass	Kg	200
Distance between rear thrust	m	1.17
<b>UUV parameters</b>		
Dimensions ( $L \times B \times H$ )	m	$1.79 \times 0.25 \times 0.25$
Weight	kg	12 (in water)
Center of gravity	m	(0, 0, 0.0196)
Center of buoyancy	m	(0, 0, 0)
Moment of inertia	$\text{kgm}^2$	(0.177, 3.45, 3.45)

- Case 1: Dynamic behavior of the USV (straight motion, turning motion with disturbance)
- Case 2: Dynamic behavior of the UUV (straight motion, turning motion with disturbance)
- Case 3: Dynamic behavior of the unmanned ocean platform (straight motion, turning motion with disturbance)

#### 4.1. Case 1: Dynamic Behavior of the USV without Disturbance

Figure 13 shows the simulation results related to the USV's straightness and turning in an environment without disturbance. The thrust force when going straight is 29.2 kgf and the thrust forces of each thruster when turning are 29.2 kgf and 14.6 kgf. Looking at the simulation results, it can

be seen that the USV has a velocity of about 0.8 m/s when in straight motion. Also, it was confirmed that it has a turning radius of about 1.75 m when turning.

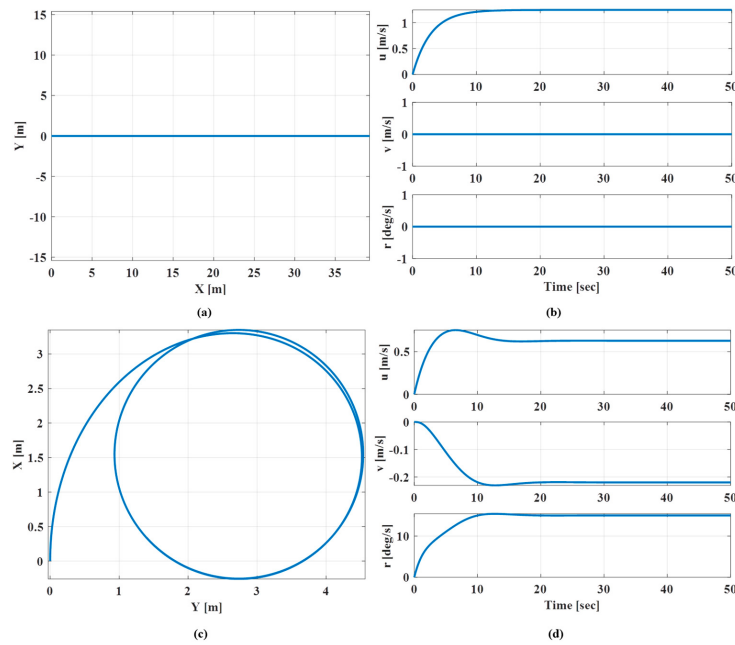


**Figure 13.** Simulation result of dynamics behavior of the USV according to straight and turning motion: (a) X-Y trajectory of the USV (straight motion); (b) Linear and angular velocity of the USV (straight motion); (c) X-Y trajectory of the USV (turning motion); (d) Linear and angular velocity of the USV (turning motion).

#### 4.2. Case 2: Dynamic Behavior of the USV with Disturbance (Wind Load, Current)

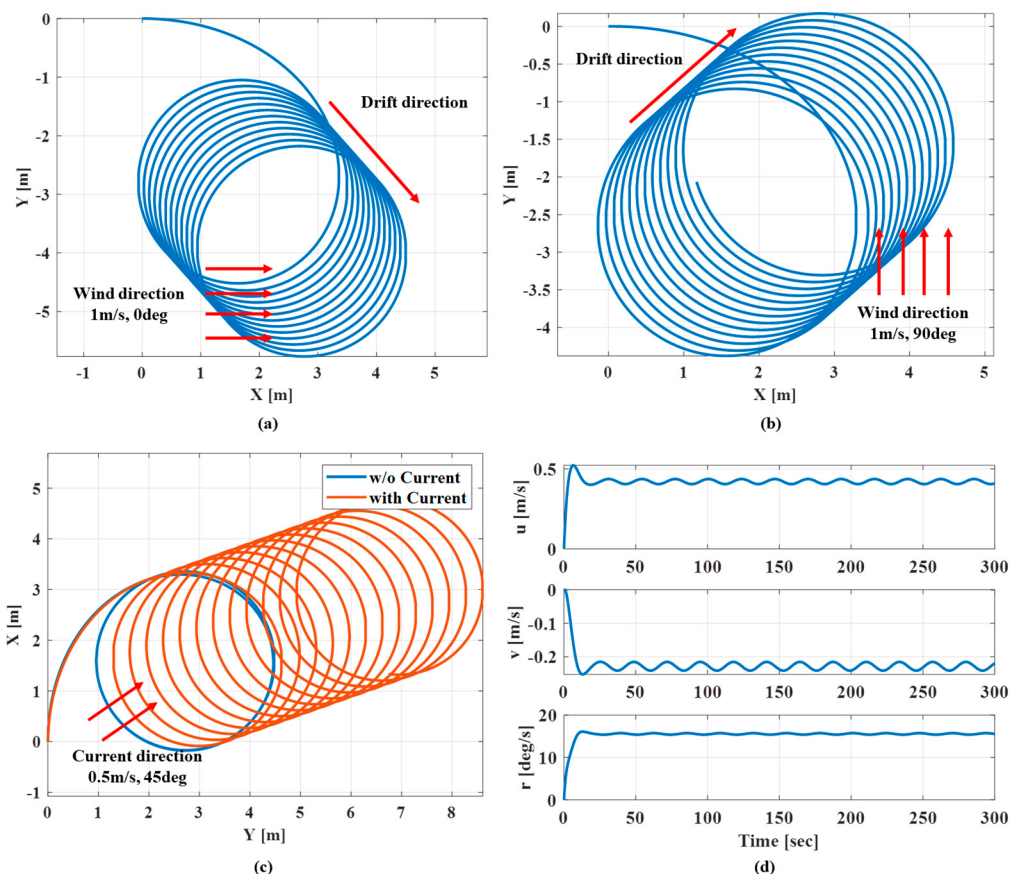
Figure 14 shows the simulation of the turning motion of an USV in an environment where wind load and current are present. In general, when confirming the validity of the wind load and current model, it is determined by using the drifting direction and distance through the turning motion rather than the straight motion of the USV. During the simulation, it was assumed that the wind load had a wind velocity of 1 m/s at 0 deg and 1 m/s at 90 deg. In addition, the current was set to have a velocity of 0.5 m/s at 45 deg. Through the current research that analyze the ship's turning performance and disturbance, the drifting direction of the ship itself drifts in an oblique direction rather than the same direction as the incident disturbance [29,30]. As can be seen from the simulation results, it can be confirmed that USV is drifted by wind and current. Also, it can be seen that the velocity stabilizes once past the initial transitional state, and through these results, it can be seen that the modeled USV and disturbances are valid.

#### 4.3. Case 3: Dynamic Behavior of the UUV

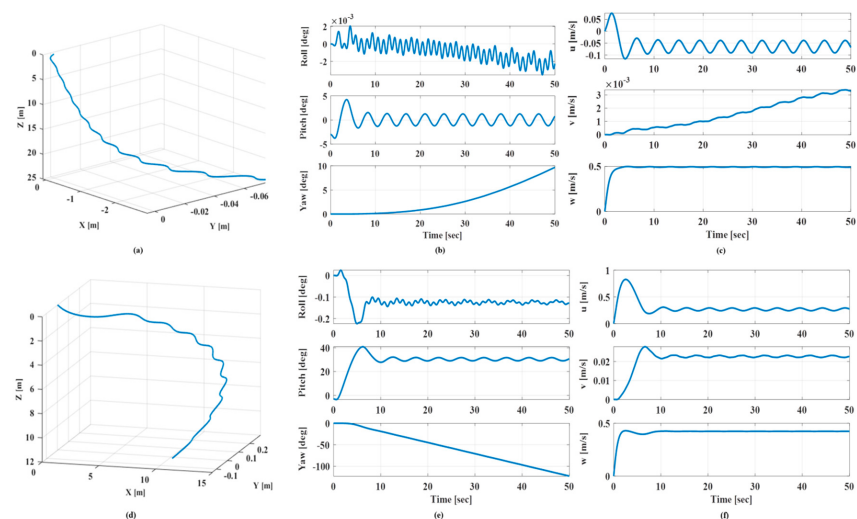
The UUV does not include a separate thruster to control the vertical force. The basic concept has the assumption that the movement in the Z-axis direction will not occur significantly in the form of a combination of a cable and a UUV having negative buoyancy. This simulation is to check the dynamic motion of UUV without a connected cable.

Figure 15a–c show the results of the UUV motion in the absence of thruster input. The UUV, having negative buoyancy, moves in the depth direction (Z-axis). Also, it can be seen that the Y-axis movement occurs as roll, pitch, and yaw angles. The graphs d–f show the result when the same input is given to the thruster mounted on the port and starboard. As in the previous graph of UUV motion in the depth direction, it can be seen in the Figure 13e that the UUV rotates as the roll passes through

the transient state and has an angle of about  $-0.1$  deg. Also, it can be seen from (f) that the velocity in the x-axis direction is increased due to the thrust forces.



**Figure 14.** Simulation results of dynamic behavior of USV with disturbance: (a) Turning motion of the USV with wind load ( $1\text{ m/s}, 0\text{ deg}$ ); (b) With wind load ( $1\text{ m/s}, 90\text{ deg}$ ); (c) With current ( $0.5\text{ m/s}, 45\text{ deg}$ ); (d) Linear and angular velocity of the USV with current ( $0.5\text{ m/s}, 45\text{ deg}$ ).



**Figure 15.** Simulation results of dynamic behavior of an UUV without disturbance: (a) X-Y and Z-X trajectory of the UUV without thrust input; (b) Euler's Angles of the UUV; (c) Linear velocity of the UUV; (d) X-Y and Z-X Trajectory of the UUV with thrust input(port and starboard:  $8.0\text{ kgf}$ ); (e) Euler's angles of the UUV; (f) Linear velocity of the UUV.

#### 4.4. Case 4: Dynamic Behavior of the UUV with Disturbance (Current)

Figure 16 shows the simulation results for the turning motion with the input applied to the UUV bow thruster. In addition, the simulation results were compared for the case of current to confirm the validity of the modeled disturbance. The input of the bow thruster was 5 kgf, and the current was set to 0.5 m/s. As in the result of the previous simulation, it can be confirmed that the UUV having negative buoyancy moves in the z-axis direction while turning. Unlike a platform that controls the turning motion of the UUV using a rudder, the thrust force of the bow thruster directly affects the turning motion of the UUV. Therefore, it can be confirmed that the turning radius is very small at 0.5 m. In the presence of current, the UUV drifts due to disturbance, and the turning radius is about 1.3 m and moves in the depth direction.

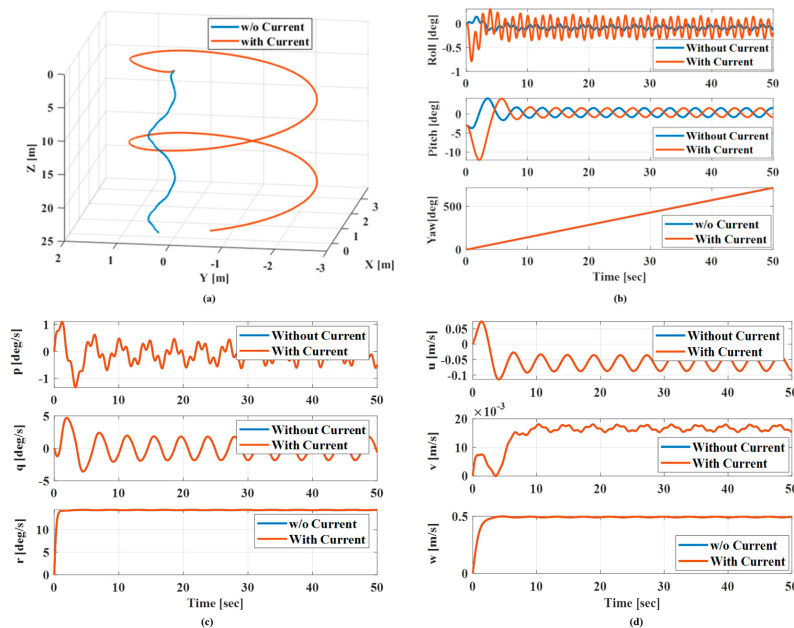


**Figure 16.** Simulation results of dynamic behavior of UUV (Blue line: without disturbance, Orange line: with disturbance): (a) X-Y-Z Trajectory of UUV when turning motion; (b) Euler’s Angles of UUV; (c,d) Linear & Angular Velocity of UUV.

As can be seen through each graph, each state of the UUV increases the vibration and initial state values by the current. In particular, since the given current is 0.5 m/s in the x-axis direction, it can be seen that the velocity in the x-axis direction of the UUV increases. Accordingly, it can be concluded that the turning radius increases. Through the previous simulation, it was confirmed that the validity of the motion equations of the USV, UUV, and underwater cable and disturbance models. Finally the dynamic behavior of the unmanned ocean platform simulation was performed to check the interaction between the underwater cable, USV, and UUV.

#### 4.5. Case 5: Dynamic Behavior of the Unmanned Ocean Platform (Stationary Motion)

The simulation performed in Case 5 analyzed the dynamic behavior of the stationary state using the entire equation of motion of the unmanned ocean platform. In the Case 5 ~ 7 simulations, it is assumed that the UUV is located 3 m in the depth direction. The actual platform will use the winch to manage the underwater cable, but the simulation did not take this into account and performed the motion analysis. In the future, we will consider underwater cable management and UUV heave motion control when creating a platform using our simulation results. Figure 17a shows the trajectory of the unmanned ocean platform in the X-Z plane. The circled mark on the graph represents each node of the underwater cable.

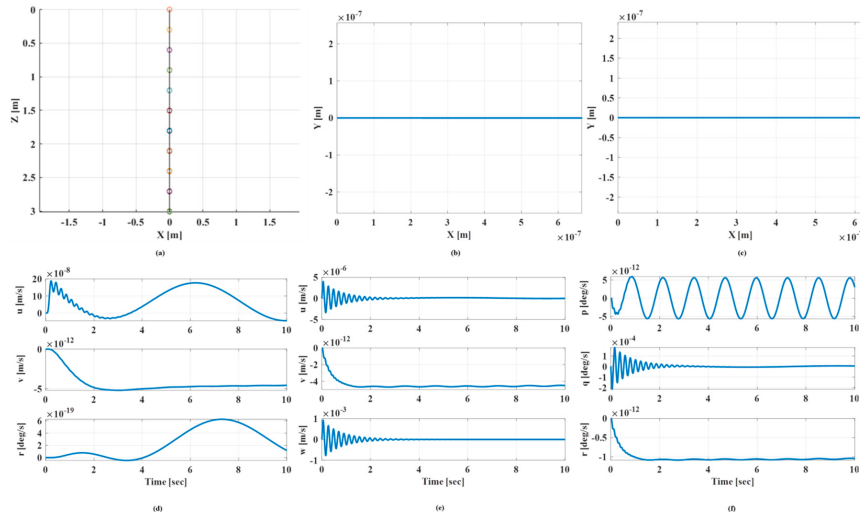


**Figure 17.** Simulation results of dynamic behavior of unmanned ocean platform when stationary motion: (a) X-Z trajectory; (b) X-Y trajectory of the USV; (c) X-Y trajectory of the UUV; (d) Linear and angular velocity of the USV; (e) Linear velocity of the UUV; (f) Angular velocity of the UUV.

The cable length is 3 m, with the USV at 0 m and UUV at 3 m. (b) and (c) show the X-Y trajectory of the USV and UUV. The size of each axis is  $10^{-7}$ , so it can be said that there is almost no movement. Also, (d–f) show the linear and angular velocity of each platform. We can see that it has a vibration, but its size is very small.

This vibration can be explained using the lumped-mass method and Figure 18. It can be seen that vibration occurs due to the interaction between each segment composed of a spring, damper and adjacent node. The force generated at both end of the underwater cable is shown in Figure 18, which shows the forces acting on the USV and UUV in a static state, and it can be seen that it has an initial vibration but stabilizes over time. Also, we can see that by looking at the force acting on the Z-axis, it shows 12N, which is equal to the weight of the UUV in water. The forces acting on the rest of the directions are negligibly small.

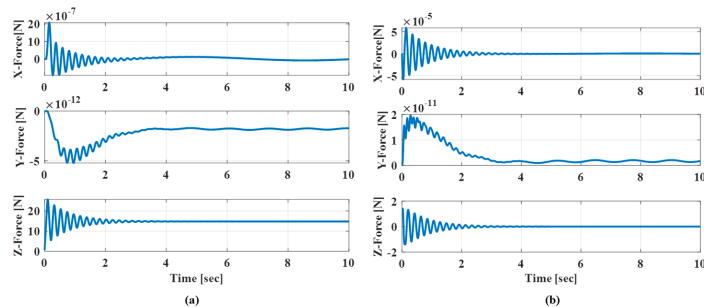


**Figure 18.** Forces by underwater cable when stationary motion: (a) Force acting on the UUV; (b) Force acting on the USV.

#### 4.6. Case 6: Dynamic Behavior of the Unmanned Ocean Platform (Similar Velocity)

The simulations in cases 6 and 7 show the interpretation of dynamic behavior when the operating velocities of the USV and UUV are the same or different. It is a simulation to check this under the assumption that if the velocity of each platform is different, the cable forces will be significantly affected.

The initial value of USV and UUV are  $[u_s, v_s, r_s] = [0, 0, 0]$  and  $[u_f, v_f, w_f, p_f, q_f, r_f] = [0, 0, 3, 0, 0, 0]$ , respectively. In order to achieve a similar velocity, input was applied to the thruster of each platform. Figure 19 shows the velocity of the X-Z plane and X-Y plane trajectory of the USV and UUV of the unmanned ocean platform. We can see that the velocity remains similar over time.

Figure 20 shows each state value of the USV and UUV, and each state value can be confirmed to move while maintaining a very small value. Figure 21 also shows the forces acting on each platform. If the velocities of the two platforms are similar, the force acting on each platform is small, so it can be seen that it does not significantly affect the state value. In particular, it can be seen that the force in the Z-axis direction acting on the UUV shows almost 0.3 N, which has little effect on the depth direction.

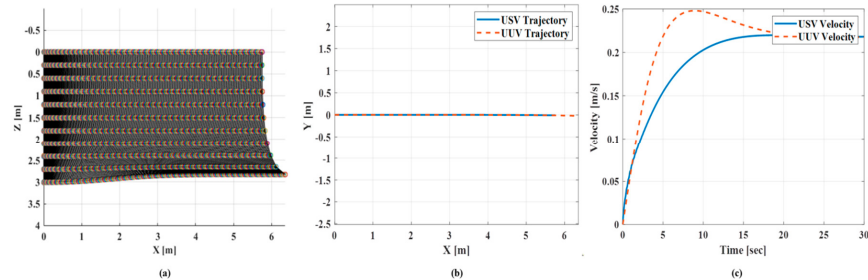


**Figure 19.** Simulation results of dynamic behavior of unmanned ocean platform when the USV and UUV velocities are similar: (a) X-Z trajectory of the unmanned ocean platform; (b) X-Y trajectory of the USV and UUV; (c) X-axis velocity of the USV and UUV.

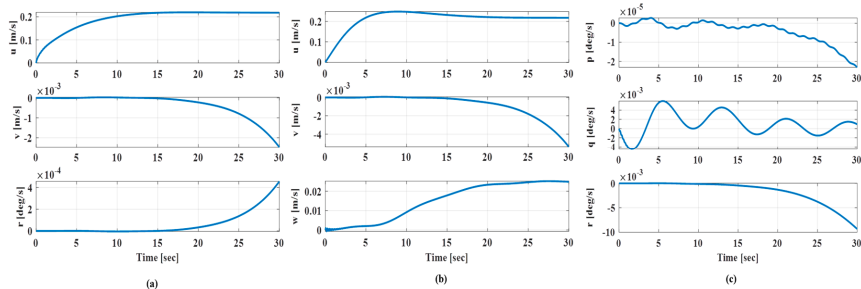


**Figure 20.** Simulation results of state values of the unmanned ocean platform: (a) Linear and angular velocity of the USV; (b) Linear velocity of the UUV; (c) Angular velocity of the UUV.

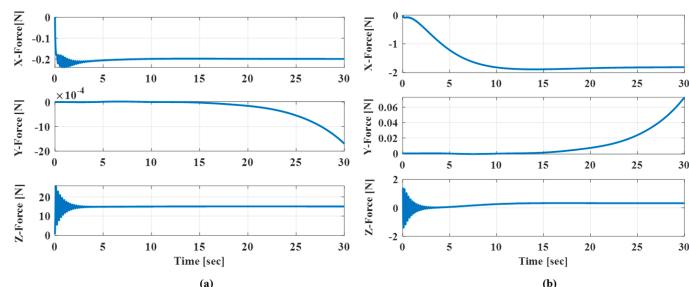


**Figure 21.** Forces generated by the underwater cable: (a) Forces acting on the USV; (b) Forces acting on the UUV.

#### 4.7. Case 7: Dynamic Behavior of the Unmanned Ocean Platform (Different Velocity)

As in Case 7, a simulation was performed by different input values of the thruster of each platform under the initial conditions. When the velocity of the USV and UUV are different, the UUV moves upwards, as shown in subfigure (a) of Figure 22. After about 15 s, we can see that the speed of each platform becomes similar. This is because the UUV is dragged by the speed difference between the USV and UUV. In addition, the X-Y trajectory of each platform, the moving speed, and the state of each axial direction can be confirmed in Figures 23 and 24. Compared to Case 6, it can be seen that the rotation speed of the Z-axis of the UUV is increased, which indicates that the straightness of the UUV is deteriorated.

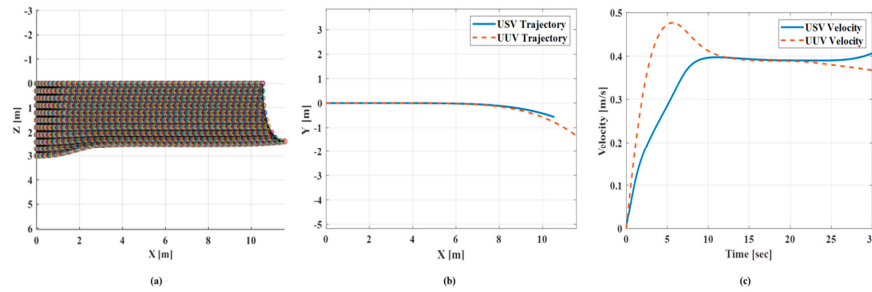


**Figure 22.** Simulation results of dynamic behavior of unmanned ocean platform when the USV and UUV velocities are different: (a) X-Z plane trajectory; (b) X-Y plane trajectory of the USV and UUV; (c) Velocity of the USV and UUV.

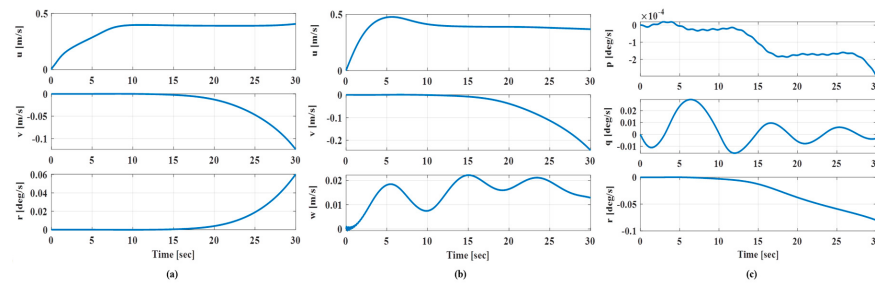


**Figure 23.** Simulation results of state values of the unmanned ocean platform: (a) Linear and angular velocity of the USV; (b) Linear velocity of the UUV; (c) Angular velocity of the UUV.

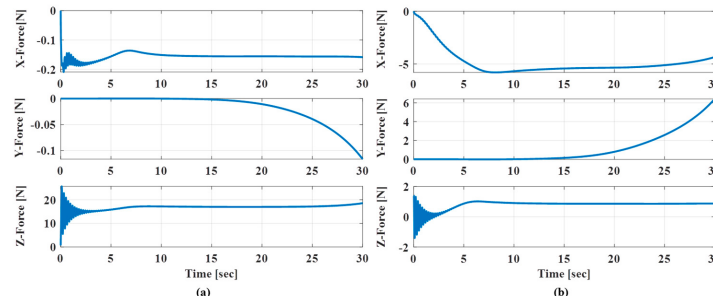


**Figure 24.** Forces generated by the underwater cable: (a) Forces acting on the USV; (b) Forces acting on the UUV.

In Figure 24 we can see that there is no significant force in the X and Y-axis directions of the USV. This is because the mass of USV is relatively large. On the other hand, the force acting on the UUV is relatively large, and as a result, the UUV does not move straight. Also, it can be seen that the UUV, which is ahead of USV due to the difference in initial speed, receives the force pulled back by the cable and rises by force in the depth direction. In conclusion, it was confirmed through simulation results that the previous assumption that the speed of each platform could be significantly affected by the cable could be confirmed.

## 5. Conclusions

This paper describes a study through derivation and simulation of motion on the dynamic behavior equations of an unmanned ocean platform in which an underwater cable connect an USV and an UUV. The motion equations of the USV and UUV are based on Newton's second law, and the underwater cable ones are developed using the lumped-mass method and Newton's second law. Also, thrust force curves of thruster to be used in the USV and UUV were derived through experiments. The derived thrust force curve was applied to the simulation to describe the motion of the actual platform well. In the dynamic behavior analysis of an unmanned ocean platform, the interaction force between the underwater cable and each platform plays a critical role. Therefore, it was confirmed that

the motion equation of the developed underwater cable and the result value through the experiment were compared and validated. Also, a motion equation was developed in consideration of wind load and current due to disturbance. Finally, the equation of motion of the unmanned ocean platform considering interaction was developed.

First, using the developed motion equations of the USV and UUV, the performance of the case with and without disturbance was confirmed. As a result of the simulation, it was confirmed that the motion was well represented. As a result of the simulation using the overall motion equation of the unmanned ocean platform, it can be seen that if there is a difference in speed between the USV and UUV, the depth of the UUV and the X-Y plane motion is affected by the force generated by the underwater cable. Also, it was confirmed that the force generated by the underwater cable also acts on the USV but it does not significantly affect the motion of the relatively large USV.

Based on the results of this study, requirements for developing a real platform could be derived. First, to minimize the effect of the underwater cable, the USV and UUV should move at a similar speed. Second, it is necessary to increase the degree of freedom of control of the UUV, which is currently capable of 3-DOF. Third, similar to the first consideration, it is necessary to control the formation of the USV and UUV to reduce the impact of the underwater cable. In the future, based on these considerations, we intend to develop a real platform and develop the related controllers and conduct field tests.

**Author Contributions:** Methodology, S.M.H. and J.-Y.K.; formal analysis and writing original draft paper, S.M.H. and K.N.H.; writing review and editing, S.M.H. and J.-Y.K.; The authors contributed equally to this work. All authors have read and agreed to the published version of the manuscript.

**Funding:** This study has been conducted with the support of the Korea Institute Technology as “The development of Intelligent Marine Robot to improve Underwater Work Convenience(kitech JA-20-0002”

**Conflicts of Interest:** The authors declare no conflict of interest.

## Appendix A

Appendix A contains the system matrix of nonlinear dynamic equation of motion.

- Inertia and Coriolis Matrix w.r.t rigid body:

$$M_{RB} = \begin{bmatrix} m & 0 & 0 & 0 & mz_g & -my_g \\ 0 & m & 0 & -mz_g & 0 & mx_g \\ 0 & 0 & m & my_g & -mx_g & 0 \\ 0 & -mz_g & my_g & I_x & -I_{xy} & -I_{xz} \\ mz_g & 0 & -mx_g & -I_{yx} & I_y & -I_{yz} \\ -my_g & mx_g & 0 & -I_{zx} & -I_{zy} & I_z \end{bmatrix} \quad (A1)$$

$$C_{RB} = \begin{bmatrix} 0 & 0 & 0 & m(y_g q + z_g r) & -m(x_g q - w) & -m(x_g r + v) \\ 0 & 0 & 0 & -m(y_g p + w) & m(z_g r + x_g p) & -m(y_g r - u) \\ 0 & 0 & 0 & -m(z_g p - v) & -m(z_g q + u) & m(x_g p + y_g q) \\ m(y_g q + z_g r) & -mz_g & my_g & 0 & -I_{yz}q - I_{xy} + I_zr & I_{yz}r + I_{xy}p - I_yq \\ m(x_g q - w) & 0 & -mx_g & I_{yz}q + I_{xy}p - I_zr & 0 & I_{yz}r - I_{xy}p - I_xq \\ m(z_g p + v) & m(y_g r - u) & -m(x_g p + x_g p) & -I_{yz}r - I_{xy}p + I_yq & I_{xy}r + I_{xy}q - I_xp & 0 \end{bmatrix} \quad (A2)$$

- Inertia Matrix (Added Mass):

$$M_A = \begin{bmatrix} -X_u & 0 & 0 & 0 & 0 & 0 \\ 0 & -Y_v & 0 & 0 & 0 & -Y_r \\ 0 & 0 & -Z_w & 0 & -Z_q & 0 \\ 0 & 0 & 0 & -K_p & 0 & 0 \\ 0 & 0 & -M_w & 0 & -M_q & 0 \\ 0 & -N_v & 0 & 0 & 0 & -N_r \end{bmatrix} \quad (\text{A3})$$

- Hydrodynamic Coriolis Matrix (Added Mass):

$$C_A(v) = \begin{bmatrix} 0 & 0 & 0 & 0 & -Z_w w & Y_v v \\ 0 & 0 & 0 & Z_w w & 0 & -X_u u \\ 0 & 0 & 0 & -Y_v v & X_u u & 0 \\ 0 & -Z_w w & Y_v v & 0 & -N_r r & M_q q \\ Z_w w 0 & 0 & -X_u u & N_r r & 0 & -K_p p \\ -Y_v v & X_u u & 0 & -M_q q & K_p p & 0 \end{bmatrix} \quad (\text{A4})$$

- Hydrodynamic Damping Matrix (Linear and Non-linear term):

$$D_l = \begin{bmatrix} -X_u & 0 & 0 & & & \\ 0 & -Y_v & 0 & & & 0_{3 \times 3} \\ 0 & 0 & -Z_w & & & \\ & & & -K_p & 0 & 0 \\ & 0_{3 \times 3} & & 0 & -M_q & 0 \\ & & & 0 & 0 & -N_r \end{bmatrix} \quad (\text{A5})$$

$$D_{nl}(v) = \begin{bmatrix} -X_{u|u}|u| & 0 & 0 & & & \\ 0 & -Y_{v|v}|v| & 0 & & & 0_{3 \times 3} \\ 0 & 0 & -Z_{w|w}|w| & & & \\ & & & -K_{p|p}|p| & 0 & 0 \\ & 0_{3 \times 3} & & 0 & -M_{q|q}|q| & 0 \\ & & & 0 & 0 & -N_{r|r}|r| \end{bmatrix} \quad (\text{A6})$$

- Restoring Forces and Moments:

$$g(\eta) = \begin{bmatrix} (W-B)\sin\theta \\ -(W-B)\cos\theta\sin\phi \\ -(W-B)\cos\theta\cos\phi \\ -(y_g W - y_b B)\cos\theta\cos\phi + (z_g W - z_b B)\cos\theta\sin\phi \\ (z_g W - z_b B)\sin\theta + (x_g W - x_b B)\cos\theta\sin\phi \\ -(x_g W - x_b B)\cos\theta\cos\phi + (y_g W - y_b B)\sin\theta \end{bmatrix} \quad (\text{A7})$$

## References

1. Ha, J.-H.; Ko, H.-K.; Cho, H.-S.; Chung, W.; Ahn, D.; Shin, S.-R. A proposal of marine geophysical exploration techniques for offshore plant installation. *J. Korean Soc. Mar. Eng.* **2013**, *37*, 242–251.
2. Marsset, T.; Marsset, B.; Ker, S.; Thomas, Y.; Le Gall, Y. High and very high resolution deep-towed seismic system: Performance and examples from deep water Geohazard studies. *Deep. Sea Res. Part I: Oceanogr. Res. Pap.* **2010**, *57*, 628–637. [CrossRef]

3. Balanzar, L.N.; Sanchez-Gaytán, J.L.; Fonseca-Navarro, F.; Salgado-Jiménez, T.; Garcia-Valdovinos, L.G.; Rubio-Lopez, O.; Gómez-Espinosa, A.; Ramirez-Martinez, A. Towards Teleoperation and Automatic Control Features of an Unmanned Surface Vessel-ROV System: Preliminary Results. In Proceedings of the 14th International Conference on Informatics in Control, Automation and Robotics, Madrid, Spain, 26–28 July 2017; pp. 292–299.
4. ECA Groups Shows Off USV/ROV Combo for Subsea IMR Ops. Available online: <https://www.ecagroup.com/media-file/5444-eca-group-press-review-subsea-world-news-eca-group-shows-off-usv-rov-combo-for-subsea-imr-ops.pdf> (accessed on 28 April 2020).
5. Available online: <https://www.unmannedsystemstechnology.com/2013/10/video-thales-asv-saab-complete-unmanned-mine-countermeasures-exercise/> (accessed on 28 April 2020).
6. Available online: [https://ndiastorage.blob.core.usgovcloudapi.net/ndia/2005/umv\\_auv/tuesday/mons.pdf](https://ndiastorage.blob.core.usgovcloudapi.net/ndia/2005/umv_auv/tuesday/mons.pdf) (accessed on 28 April 2020).
7. Kamman, J.W.; Huston, R.L. Modeling of Variable Length Towed and Tethered Cable Systems. *J. Guid. Control. Dyn.* **1999**, *22*, 602–608. [CrossRef]
8. Masciola, M.; Jonkman, J.; Robertson, A. Extending the capabilities of the mooring analysis program: A survey of dynamic mooring line theories for integration into FAST. In Proceedings of the ASME 2014 3rd International Conference on Ocean, Offshore and Arctic Engineering, San Francisco, CA, USA, 8–13 June 2014.
9. Eidsvik, O.A.N.; Schjølberg, I. Finite element cable-model for Remotely Operated Vehicles (ROVs) by application of beam theory. *Ocean Eng.* **2018**, *163*, 32–36.
10. Driscoll, F.R.; Lueck, R.G.; Nahon, M. Development and validation of a lumped-mas dynamics model of a dep-sea ROV system. *Appl. Ocean Res.* **2000**, *22*, 169–182. [CrossRef]
11. Buckham, B.J. Dynamics Modeling of Low-Tension Tethers for Submerged Remotely Operated Vehicles. Master’s Thesis, University of Victoria, Victoria, BC, Canada, 2011.
12. Merchant, H.C.; Kelf, M.A. Non-Linear Analysis of Submerged Ocean Buoy Systems. In Proceedings of the Ocean 73—IEEE International Conference on Engineering in the Ocean Environment, Seattle, WA, USA, 25–28 September 1973; Volume 1, pp. 390–395.
13. Choo, Y.-I.; Casarella, M.J. A Survey of Analytical Methods for Dynamic Simulation of Cable-Body Systems. *J. Hydraulics* **1973**, *7*, 137–144. [CrossRef]
14. Grosenbaugh, M. Transient behavior of towed cable systems during ship turning maneuvers. *Ocean Eng.* **2007**, *34*, 1532–1542. [CrossRef]
15. Fossen, T.I. *Guidance and Control of Ocean Vehicles*; Wiley: New York, NY, USA, 1994; Volume 199.
16. Muske, K.R.; Ashrafiou, H.; Haas, G.; McCloskey, R.; Flynn, T. Identification of a control oriented nonlinear dynamic USV model. In Proceedings of the 2008 American Control Conference, Seattle, WA, USA, 11–13 June 2008; pp. 562–567.
17. Gertler, M.; Hagen, G.R. *Standard Equations of Motion for Submarine Simulation*; No. NSRDC-2510; David w Taylor Naval Ship Research and Development Center Bethesda MD: Washington, USA, 1967.
18. *Advances in Unmanned Marine Vehicles*; Roberts, G.N.; Robert, S. (Eds.) IET: Stevenage, UK, 2006; Volume 69.
19. Prestero, T.J. Verification of a Six-Degree of Freedom Simulation Model for the REMUS Autonomous Underwater Vehicle. Ph.D. Thesis, Massachusetts Institute of Technology, Cambridge, MA, USA, 2001.
20. Buckham, B.; Nahon, M.; Seto, M.; Zhao, X.; Lambert, C. Dynamics and control of a towed underwater vehicle system, part I: Model development. *Ocean Eng.* **2003**, *30*, 453–470. [CrossRef]
21. Available online: <https://minnkotamotors.johnsonoutdoors.com/saltwater-trolling-motors/riptide-engine-mount> (accessed on 28 April 2020).
22. Available online: <https://tecnadyne.com/wp-content/uploads/2017/06/Model-300-Brochure-3.pdf> (accessed on 28 April 2020).
23. Huang, S. Dynamic analysis of three-dimensional marine cables. *Ocean Eng.* **1994**, *21*, 587–605. [CrossRef]
24. Kelf, M.; Merchant, H. Analysis of a multiple buoy instrument platform; A non linear model. In Proceedings of the Ocean '74—IEEE International Conference on Engineering in the Ocean Environment, Halifax, NS, Canada, 21–23 August 1974; Volume 1, pp. 4–48.
25. Thomson, W.T.; Dahleh, M.D. *Theory of Vibrations with Applications*; Prentice Hall: Upper Saddle River, NJ, USA, 1982; pp. 16–89.
26. Driscoll, F.R.; Nahon, M. Mathematical Modeling and Simulation of a Moored Buoy System. In Proceedings of the MTS/IEEE OCEANS '96, Fort Lauderdale, FL, USA, 23–26 September 1996; Volume 1, pp. 517–523.

27. Newman, J.N. *Marine Hydrodynamics*; MIT Press: Cambridge, MA, USA, 1977.
28. Reyhanoglu, M. Control and stabilization of an underactuated surface vessel. In Proceedings of the 35th IEEE Conference on Decision and Control, Kobe, Japan, 13–14 December 1996; Volume 3.
29. Ueno, M.; Nimura, T.; Miyazaki, H. Experimental study on maneuvering motion of a ship in waves. In Proceedings of the International Conference on Marine Simulation and Ship Maneuverability, Kanazawa, Japan, 25–28 August 2003.
30. Yasukawa, H. Simulations of a ship maneuvering in waves (1st report: Turning motion). *J. Jpn. Soc. Nav. Archit. Ocean Eng.* **2006**, *4*, 127–136. [[CrossRef](#)]



© 2020 by the authors. Licensee MDPI, Basel, Switzerland. This article is an open access article distributed under the terms and conditions of the Creative Commons Attribution (CC BY) license (<http://creativecommons.org/licenses/by/4.0/>).